Mechanism of Sulfide Binding by Ferric Hemeproteins

Fernando M. Boubeta,[†,#] Silvina A. Bieza,[†,#] Mauro Bringas,[†,‡] Darío A. Estrin,[†,‡] Leonardo Boechi,[§] and Sara E. Bari*[†]

†Instituto de Química Física de los Materiales, Medio Ambiente y Energía (INQUIMAE), CONICET and Universidad de Buenos Aires, Buenos Aires 1053, Argentina

‡Departamento de Química Inorgánica, Analítica y Química Física and §Instituto de Cálculo, Facultad de Ciencias Exactas y Naturales, Universidad de Buenos Aires, Buenos Aires 1053, Argentina

S *Supporting Information*

ABSTRACT: The reaction of hydrogen sulfide (H_2S) with hemeproteins is a key physiological reaction; still, its mechanism and implications are not completely understood. In this work, we propose a combination of experimental and theoretical tools to shed light on the reaction in model system microperoxidase 11 (MP11-Fe^{III}) and myoglobin (Mb-Fe^{III}), from the estimation of the intrinsic binding constants of the species H_2S and hydrosulfide (HS^-), and the computational description of the overall binding process. Our results show that H_2S and HS^- are the main reactive species in Mb-Fe^{III} and MP11-Fe^{III}, respectively, and that the magnitude of their intrinsic binding constants are similar to most of the binding constants reported so far for hemeproteins systems and model compounds. However, while the binding of HS^- to Mb-Fe^{III} was negligible, the binding of H_2S to MP11-Fe^{III} was significant, providing a frame for a discriminated analysis of both species and revealing differential mechanistic aspects. A joint inspection of the kinetic data and the free energy profiles of the binding processes suggests that a dissociative mechanism with the release of a coordinated water molecule as rate limiting step is operative in the binding of H_2S to Mb-Fe^{III} and that the binding of HS^- is prevented in the access to the protein matrix. For the MP11-Fe^{III} case, where no access restrictions for the ligands are present, an associative component in the mechanism seems to be operative. Overall, the results suggest that if accessing the active site then both H_2S and HS^- are capable of binding a ferric heme moiety.
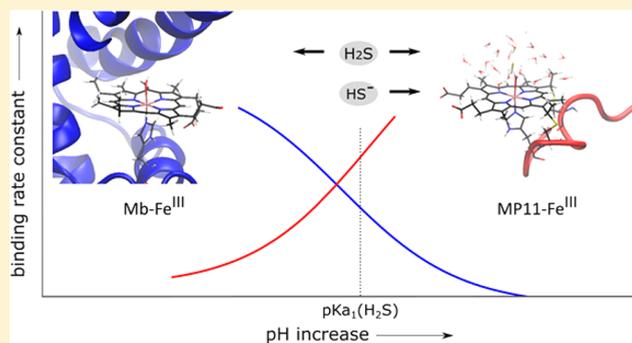
■ INTRODUCTION

The reaction of hydrogen sulfide with the heme group of hemeproteins has been associated with deleterious processes, storage, or detoxification of sulfide, promoting studies on the chemical determinants of the interaction. The metal-centered reduction of heme compounds by inorganic sulfide species,[1] readily takes place in free ferric porphyrinates[2] but is prevented in certain hemeproteins where coordination is the main outcome. The case of hemoglobin HbI from the clam *Lucina pectinata* that binds sulfide with high affinity has been considered a means for sulfide storage in organisms that live in sulfide rich muds.[3] More recently, the binding of sulfide with very high affinity has been reported for the hemoglobin from the aerobic bacteria *Vitreoscilla*.[4] Also, the binding of hydrogen sulfide to human methemoglobin and metmyoglobin (Mb-Fe^{III}) has been reported, associated with the onset of a sulfide detoxification process yielding thiosulfate and polysulfides, thus ascribing to these hemeproteins an alternative function.[5,6]

The rate constants for the binding (k_{on}) and release (k_{off}) of sulfide to ferric hemeproteins have been reported in more than 40 examples up to date, considering wild type proteins, mutants and heme model compounds (Supporting Information section SI1). For k_{on}, values close to 10^4 M^{-1} s^{-1} have been reported for most of the studied cases. In the case of myoglobin, the HisE7 is often regarded as a gate with steric control for the access of ligands, thus affecting k_{on}. However, this was shown to be inoperative for the case of dioxygen that showed little or no barrier to access the distal cavity even in the closed HisE7 conformation.[7] Unlike k_{on}, k_{off} exhibits values in a wider range, which impacts the kinetically derived affinity constant, $K_{aff} = k_{on}/k_{off}$. These affinities have been largely explained in terms of distal mechanisms.[8,9] It has been proposed that the presence of the GlnE7 typical of bacterial hemoglobins, in the distal cavity of the HbI of *Lucina pectinata* provides stabilization to the ligand by formation of a hydrogen bond,[10] strongly lowering the k_{off}.[8] Although the GlnE7 has also been observed in the hemoglobin from *Vitreoscilla*, in this case it has been attributed to the distinctive LeuE11 the control of the accessibility of the ligand to the binding site, lowering the binding affinity; in contrast, the bulky TyrB10 in the exit from the distal heme pocket has been regarded as a

steric barrier for bound sulfide from escaping, hence decreasing k_{off}. In mammalian hemoglobins, the presence of a HisE7 has also been found to play a key role in determining k_{off} and affinity.

More recently, the proximal contribution to sulfide affinity for heme compounds has been dissected and evaluated. The lowest affinity values reported to date, about $10^4 - 10^3$ M^{-1} have been measured in heme model compounds, with histidine, pyridine, or imidazole as the fifth ligands,[11−13] but lacking of distal mechanisms for ligand stabilization. These results support that the coordination of sulfide to Fe^{III} heme compounds; hence, the delay in the metal centered reduction is possible with the assistance of proximal mechanisms as a minimum requirement.

The kinetic analyses should be extended for a comprehensive evaluation of the binding of the sulfide species to hemeproteins, by adding to the description the migration of inorganic sulfide species from the bulk into the active site[14−16] and the ionization degree of the bound water molecule and of other ionizable groups in the heme moiety and/or in the surrounding residues. Particularly, protein tunnels are structures lined by amino acidic residues defining the formation of protein cavities, which may in turn act as ligand hosts,[17−21] and thus participate in the overall binding process. Additionally, the rupture of the Fe^{III}−OH$_2$ bond, typically present in many ferric hemeproteins, imposes an additional barrier.[17,22−25] Similar studies have been previously reported for other small ligands.[26]

The final product of the process, Fe^{III}−S(sulfide) bond formation, has been assessed by resonance Raman and EPR in many examples, but the protonation could not be elucidated by these techniques.[3,12,27,28] Nevertheless, the protonation states of the reactive species of sulfide have been tentatively assumed in different hemeproteins. Differing from the case of cyanide species HCN/CN$^-$ where only the deprotonated species is active for coordination to ferric heme compounds,[29,30] both the neutral and monoanionic forms of sulfide have been regarded as potential species participating in mechanistic proposals under biorelevant conditions.[5,6,8,31] Studies with picket-fence ferric porphyrinates in organic media, using gaseous H$_2$S or NBu$_4$SH as sources of the neutral and monoprotonated species, revealed that H$_2$S did not bind to the ferric compounds. The hydrosulfide, instead reduced the ferric porphyrinates and eventually bound to the ferrous forms.[32]

The decrease of k_{on} in the binding of inorganic sulfide as pH increases from 5.5 to 6 to 8−9 has been reported for HbI, II, and III from *Lucina pectinata*,[3] human and porcine hemoglobins,[5,33,34] myoglobin,[6,33,34] and *Vitreoscilla* hemoglobin,[4] suggesting that the neutral H$_2$S is the fastest reactive species. Very recent measurements of binding of H$_2$S at different pH values to human hemoglobin and horse myoglobin suggested that the only species able to react was H$_2$S, and intrinsic H$_2$S rate constants (pH independent) were reported for both cases.[33] A direct experimental evaluation of HS$^-$ reactivity toward ferric heme systems, and a comparative analysis of the reaction mechanisms of both species have not been reported so far.

An analysis for the binding of sulfide species to the HbI from *Lucina pectinata* by means of computational methods has been reported by our group, covering the process since the migration of the ligand from the bulk to the active site, to the protonation state of the bound species.[10] Initially, the migration of H$_2$S from the bulk to the binding site surpasses that of the HS$^-$. As a consequence, H$_2$S appears as the fastest species that coordinates to the metal center. The restrictions for HS$^-$ have been interpreted in terms of the higher desolvation cost for the anion, prior to the migration as free species. The theoretical calculations also suggested that water molecules assist the deprotonation process of the coordinated H$_2$S, forming a Fe^{III}(SH$^-$) complex. Although further deprotonation forming the Fe^{III}(S^{2-}) complex could not be disregarded from the analysis, the study reveals the participation of H$_2$S as migrating and reactive species, and mainly of HS$^-$ as the stabilized bound species.

A close-up inspection of the bound species electronic description was performed for the case of myoglobin, combining theoretical and spectroscopic results.[6] The first intermediate in the detoxification of sulfide mediated by metmyoglobin was described as a low-spin Fe^{III}(SH$^-$) complex, a species in which reactivity has been interpreted by means of the contribution from the Fe^{II}(SH·) resonance structure.

Overall, the behavior of inorganic sulfide toward each hemeprotein or heme compound is the result of multiple determinants and reflects the intrinsic reactivity of each sulfide species toward the Fe^{III} center. In the present study, we focused on the kinetic analysis of the binding mechanism in the reaction of sulfide toward bis-*N*-acetyl-microperoxidase **11**, ferric form, (NAcMP11-Fe^{III}, Supporting Information section SI2),[11] and to Mb-Fe^{III} as a function of pH, using complementary experimental and theoretical approaches. The cases selected are representative of two limiting scenarios: While the access of ligands to the active site of the Mb-Fe^{III} is restricted by the topology of the protein matrix, the access to the NAcMP11-Fe^{III} active site is only restricted by the presence of a water molecule as sixth ligand (p$K_{\text{H}_2\text{O/OH}^-}$ = 9.56).[35] The combined analysis of the process for the two heme systems selected allows the dissection of the determinants for a comprehensive description of the binding process of sulfide species to ferric hemeproteins.

■ EXPERIMENTAL SECTION

Materials. All chemicals were of the highest purity available and were purchased from Sigma-Aldrich. Buffers were prepared with deionized water, containing DTPA (10^{-4} M). All experiments were performed using freshly prepared solutions of anhydrous Na$_2$S (Sigma-Aldrich, >98%, tested with iodine-starch method), which was stored in a glovebox under nitrogen (<1 ppm of O$_2$ and <1 ppm of H$_2$O). Microperoxidase **11**, ferric form (MP11-Fe^{III}) was treated with acetic anhydride, forming NAcMP11-Fe^{III}, to prevent aggregation.[36] The concentrations of the solutions of Mb-Fe^{III} (from equine skeletal muscle) and of NAcMP11-Fe^{III} were determined using the extinction coefficients of 188 000 M^{-1} cm^{-1} at 409 nm, and 148 000 M^{-1} cm^{-1} at 398 nm, respectively.[6,37] The concentrations of the sulfide solutions were assessed prior to use using the iodine-starch titration method.

Kinetic Analysis. *General Procedures.* Kinetic data were obtained by recording time-resolved UV−vis spectra using a SFM-300 Bio-Logic stopped-flow module equipped with a J&M TIDAS high-speed diode array spectrometer, with combined deuterium and tungsten lamps (200−1015 nm wavelength range). For the estimation of k_{on}, the solutions of Na$_2$S were prepared by the addition of argon-saturated phosphate buffers to the argon-purged solid material in containers with silicone septa and used within a day; the solutions of Mb-Fe^{III} and NAcMP11-Fe^{III} were also exhaustively purged with argon. Solutions were delivered through anaerobic ports, using PTFE cannulas. The syringes were located in an anaerobic chamber, electronically controlled by three separate drives for the variation of

the ratio of the reagents, and thermalized at 25 °C. The system was operated using Bio-Kine 4.50 software. At least four kinetic runs were recorded for each experimental condition, and the reported data correspond to the mean values and standard deviations. All kinetic measurements were carried out under pseudo-first-order conditions unless otherwise stated. In the kinetic traces, $\Delta A = (A(t) - A_\infty)/(A_0 - A_\infty)$, where $A(t)$ is the time-dependent absorbance, A_∞ is the asymptotic value of the absorbance taken from the exponential fit, and A_0 is the initial value of absorbance. The reactions were studied at an ionic strength of 0.5 M (buffer PO_4^{3-}, varying pH); pH was measured with a calibrated Hanna precision pH meter Model 211.

Binding Kinetics of Sulfide to Mb-Fe^{III}. The dependence of the rate constant of the interaction between Mb-Fe^{III} and Na$_2$S with pH solutions of varying concentrations was determined by rapid mixing the solution of 10^{-5} M Mb-Fe^{III} at pH from 6.30 to 8.00 with the Na$_2$S solutions from 10^{-3} to 10^{-2} M at each pH. The decrease of the 409 nm signal was followed at 25 °C. The total observation time for each measurement was 1 s. The dead time was 3 ms. The data were best fitted to single exponential functions of the complete kinetic traces using the software Mathematica,[38] to obtain the observed rate constants k_{obs}. From the slope of the linear fit of the dependence of k_{obs} versus [Na$_2$S], an estimate of the kinetic binding constant, k_{on}, was derived. Each data set is represented by the average of at least four independent measurements, and the corresponding standard deviation.

Binding Kinetics of Sulfide to NAcMP11-Fe^{III}. The dependence of the rate constant of the interaction between NAcMP11-Fe^{III} and Na$_2$S solutions of varying concentrations was determined by rapid mixing the solution of 10^{-5} M NAcMP11Fe^{III} at pH from 5.6 to 7.1 with the Na$_2$S solutions with concentrations from 10^{-4} to 10^{-3} M at each pH. The decrease of the 398 nm signal was followed at 25 °C. The total observation time for each measurement was 4 s, and the dead time was 2 ms. The data were fitted to double exponential functions of the complete kinetic traces using the software Mathematica,[38] to obtain the observed rate constants k_{obs}, from the fast process. From the slope of the linear fit of the dependence of k_{obs} versus [Na$_2$S], an estimate of the kinetic binding constant, k_{on}, was derived.

The intrinsic rate constants of binding of H$_2$S and HS$^-$ for Mb-Fe^{III} and NAcMP11-Fe^{III} were calculated from the global fits of k_{on} versus pH values. Under this model, it was assumed that only the conjugate species H$_2$S and HS$^-$ are reactive:

$$k_{on} = k_{int}^{H_2S}\alpha[H_2S] + k_{int}^{HS^-}\alpha[HS^-] \quad (1)$$

where $\alpha[H_2S]$ and $\alpha[HS^-]$ are the dissociation degrees [H$_2$S]/[S]total and [HS$^-$]/[S]total, respectively.

The intrinsic rate constants for the binding of H$_2$S and HS$^-$, $k_{int}^{H_2S}$ and $k_{int}^{HS^-}$, were calculated from the global fits of k_{on} versus pH values. In terms of the dissociation constant of H$_2$S and pH, eq 1 takes the following form:

$$k_{on} = \frac{k_{int}^{H_2S}\cdot 10^{-pH}}{(K_a + 10^{-pH})} + \frac{k_{int}^{HS^-}\cdot K_a}{(K_a + 10^{-pH})} \quad (2)$$

Computational Methods. *Preparation of the Systems and MD Simulation Parameters.* The initial structure of Mb-Fe^{III} was constructed from the X-ray structure file corresponding to Protein Databank ID 1WLA. The protonation states of amino acids were those corresponding to physiological pH (i.e., Asp and Glu negatively charged, Lys and Arg positively charged); all solvent-exposed His were protonated at the δ-N atom, as well as the proximal His coordinated to the heme iron. Crystallographic water molecules were deleted manually, and the system was solvated by constructing an octahedral box of 10 Å. Approximately 5700 TIP3P water molecules were placed inside the box through the standard criteria procedure of Amber Tools Package.[39] The structure of MP11-Fe^{III} was derived from the crystal structure of cytochrome c and conveniently truncated in order to obtain the undecapeptide. For both cases, a water molecule was added to the sixth coordination position.

Solvation was modeled by constructing a 10 Å octahedral box using the TIP3P model for water. Parameters for all residues, including both Mb-Fe^{III} and MP11-Fe^{III} were taken from the AMBER ff99SB force field,[40] except for the heme group. To obtain representative AMBER parameters of the heme group for the MD simulations, we used a heme model system devoid of peripheral substituents but with an imidazole ring and a water molecule as fifth and sixth ligands, respectively. Full QM geometry optimization was performed for the complex under DFT approximation using Gaussian03 program.[41] DFT calculations have been extensively applied to metalloproteins in general and to iron-porphyrin systems in particular.[42−46] The DFT calculations reported in this article employed PBE for both correlation and exchange functional developed by Perdew, Burke, and Ernzerhof and 6-31G** as basis sets.[47] In the optimization procedure, frequency calculations using normal mode approximation were performed to check that a local minimum in the potential energy surface was obtained. In this work, the total charge and electronic spin for the sixth coordinated complex has been fixed as ferric high spin ($S = 5/2$).

Bond angles and torsional parameters including Fe atom and sulfide species, were obtained from the full QM-optimized structures by scanning the potential energy surface around the minimum of the coordinate of interest. The resulting energy profiles were fit to the appropriate AMBER potential functional form. We used the parameters previously obtained in our group for other heme systems.[45,48] Partial atomic charges were obtained using the Restrained Electrostatic Potential Procedure (RESP) for the optimized systems, from single-point PBE/6-31G** calculations. This procedure was validated and used in several hemeproteins studies in our group.[49−51] All MD simulations were performed using periodic boundary conditions with a 9 Å cutoff and particle mesh Ewald (PME) summation method for treating the electrostatic interactions. The covalent bonds involving hydrogen atoms were restrained at their equilibrium distance by using the SHAKE algorithm, while temperature and volume where kept constant with Berendsen thermostat, as implemented in the AMBER14 package.

For both systems the equilibration protocol consisted of (i) slow heating the whole system (protein and solvation box) from 0 to 300 K for 2 ns at constant volume, with harmonic restraints of 100 kcal/mol Å² for all α-C atoms in the first nanosecond, (ii) constant pressure MD run to adjust density, and (iii) unconstrained molecular dynamics simulation during approximately ∼200 ns at constant temperature (300 K) and volume, in order to obtain systems described by the NVT ensemble. Mb-Fe^{III} structures were found to be stable during the time scale of simulations. MP11-Fe^{III} structures were also stable during the simulations, and no distal mechanisms of stabilization were observed for the sixth coordinated water molecule.[11]

Steered Molecular Dynamics (sMD). sMD is used to force the system to explore a defined transformation coordinate (ξ), usually by modifying the original description of the Hamiltonian with the addition of a harmonic guiding potential over the selected ξ. This potential is described as a spring, and characterized by its constant and center. In order to cover the relevant region of the transformation coordinate, the center of the spring is translated at an arbitrary and constant velocity (v).

In the forced system, starting from N different initial micro-configurations described by a convenient ensemble, it is possible to calculate the accumulated work for the N independent non-equilibrium change processes by sampling the transformation coordinate chosen from an initial to a final value, according to the guiding potential and velocity. With this information, it is possible to employ Jarzynski's equality (JE, eq 3) to obtain an estimation of the free energy profile of the process along the chosen transformation coordinate.

$$e^{[-\beta\cdot\Delta F(\xi)]} = \langle e^{[-\beta\cdot w_i(\xi,v)]}\rangle_N \quad (3)$$

where $\Delta F(\xi)$ is the free energy change associated with each transformation coordinate, $\beta = (k_B\cdot T)^{-1}$, k_B is the Boltzmann constant, T is the absolute temperature, and the average is performed over N independent pulling trajectories. As the free energy is obtained

from an expected value, the estimation converges after using sufficient independent work data. A convergence analysis of the free energy profiles thus is a crucial issue. A detailed description of the convergence analyses of the free energy profiles for the migration of H_2S and HS^- to Mb-Fe^{III} and MP11-Fe^{III} is presented in Supporting Information section SI4.

We evaluated the free energy profile of H_2S and HS^- along the E7 tunnel of Mb-Fe^{III} choosing the Fe–S distance as the transformation coordinate. The E7 tunnel was considered the main access to the active site in Mb-Fe^{III}. Unrestricted migration from the bulk solvent to the active heme site was considered for the MP11-Fe^{III} case. We selected a snapshot from the MD productions of the Mb-Fe^{III} state of the protein in which the H_2S (or HS^-) was located at 12 Å from the heme iron. The position was chosen to ensure that the ligand was at the entrance of the E7 tunnel. Initial restrained MD (500 ns with H_2S and HS^-, respectively) runs were performed with the ligand position fixed at that initial value of the transformation coordinate using a 300 kcal/(mol Å²) harmonic constant, and using the same parameters for the MD described in the Steered Molecular Dynamics (sMD) section. We obtained approximately 400 uncorrelated initial snapshots, one per each nanosecond of the previously described simulation. Snapshots in which the ligand is not properly located to access the distal pocket were discarded. For MP11-Fe^{III}, we selected a snapshot from the MD production for which the H_2S (or HS^-) was located at 10 Å from the heme iron toward the metal center, on the distal side. Initial restrained MD (150 ns with H_2S and HS^-, respectively) runs were performed with the ligand position fixed at that initial value of the transformation coordinate using a harmonic constant of 300 kcal/(mol. Å) and using the same parameters for the MD as those described in the Steered Molecular Dynamics (sMD) section. We obtained approximately 74 and 116 uncorrelated initial snapshots for H_2S and HS^-, respectively. Snapshots in which the ligand is not properly located onto the plane of the heme group were discarded.

For both systems, the suitable initial structures were used to perform the sMD, varying the transformation coordinate from the initial distance toward 4.5 Å, using a spring constant of 300 kcal/(mol Å²) and using a pulling velocity of 0.0025 Å/ps. Spring constant and pulling velocity for the sMD simulations were similar to the computational scheme reported in previous studies.[10,52−54] In this case, the pulling velocities were chosen to be ten times slower than in previous works, in order to improve the convergence. A set of approximately 270 and 74 work profiles for H_2S and 235 and 85 work profiles for HS^- for Mb-Fe^{III} and MP-Fe^{III}, respectively, were obtained for the analysis. JE was then evaluated at each value of the transformation coordinate and the free energy profiles were estimated from eq 3.

HOMO Energies. HOMO energies were estimated from density functional theory (DFT) single point calculations for optimized geometries, using the ωB97X-D hybrid functional,[55] and G-31+G(d) basis set. The polarizable continuum model (PCM) model was used for the implicit solvation scheme.

■ RESULTS AND DISCUSSION

The reactions of Na_2S solutions toward Mb-Fe^{III} and NAcMP11-Fe^{III} at varying pH were studied under stopped flow conditions (Figure SI3). Variation of pH was intended to modulate the ratio of the inorganic sulfide species hydrogen sulfide (H_2S) and hydrosulfide (HS^-) (pK_{a1} = 6.8), in order to evaluate the binding of each species. The second deprotonation, HS^-/S^{2-}, is characterized by a pK_{a2} > 12,[56] and it was excluded from the study as the alkaline media promotes protein denaturation, and also different reactions of sulfide and the heme compounds, e.g., formation of polysulfides and sulfur.[57] In addition, the pH interval for each case was selected as a compromise with acid−base processes of structural moieties involved or expectedly involved in the binding event. For Mb-Fe^{II}, it is already known that k_{on} is modified as a function of the pH, even for ligands like CO or O_2 with no

acid−base behavior. In these cases, the k_{on} is mostly affected between pH 3 and 5, with a ca. 30 fold decrease in the value of k_{on}.[58] These changes have been ascribed to the protonation state of the distal histidine, and similar fluctuations are expected for Mb-Fe^{III}. No significant changes were observed above pH 6.

Figure 1A shows the variation of the decay of Mb-Fe^{III} as a function of pH, after rapid mixing with Na_2S solution ([Mb-
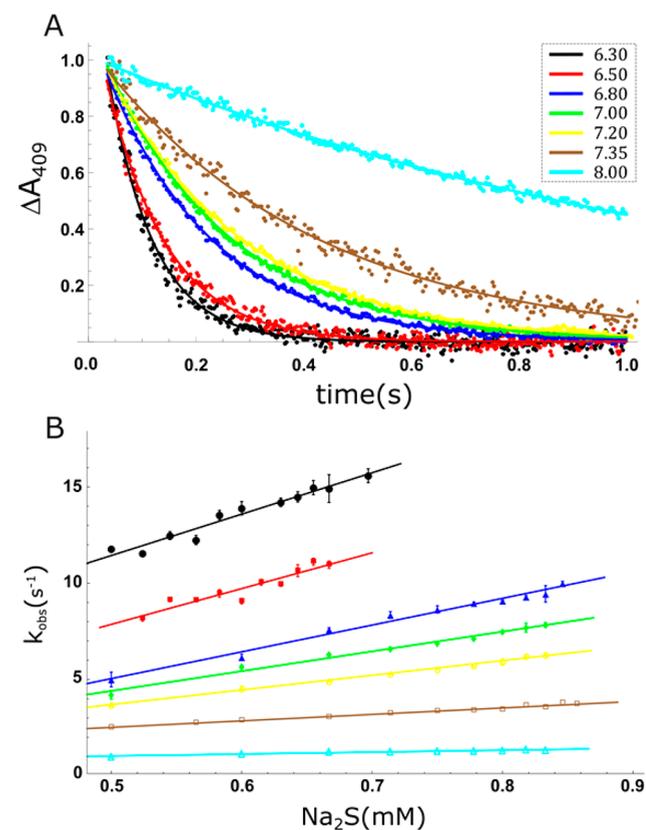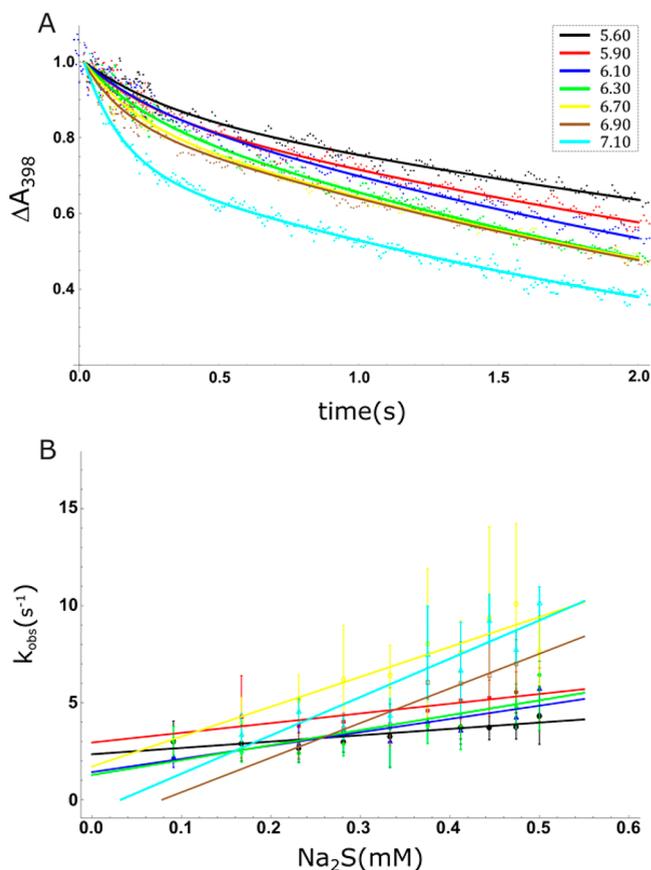

Figure 1. Mb-Fe^{III}-sulfide complex formation as a function of pH. (A) Representative stopped flow measurements at λ_{max} = 409 nm. (B) k_{obs} as a function of Na_2S concentration. The k_{on} values at each pH are obtained from the slopes of each linear dependence; the k_{on} (in M^{-1} s^{-1}) values obtained are $(2.1 \pm 0.2) \times 10^4$ at pH 6.30 (black circles), $(1.8 \pm 0.2) \times 10^4$ at pH 6.50 (red squares), $(1.40 \pm 0.07) \times 10^4$ at pH 6.80 (blue triangles), $(1.0 \pm 0.1) \times 10^4$ at pH 7.00 (green small circles), $(0.76 \pm 0.02) \times 10^4$ at pH 7.20 (yellow empty squares), $(0.34 \pm 0.01) \times 10^4$ at pH 7.35 (brown empty circles), and $(0.101 \pm 0.009) \times 10^4$ at pH 8.00 (cyan empty triangles).

Fe^{III}]:[S] = 1:100). The fitting with a single exponential decay, applied to each complete data set, retrieved the values of k_{obs}. The binding constants, k_{on}, were then estimated from the slopes of the linear plots of k_{obs} as a function of increasing concentrations of Na_2S solutions (Figure 1B), under pseudo first order conditions.

Figure 1A shows that the rate of the absorbance decay at the maximum for Mb-Fe^{III} decreases as pH is increased from 6.30 to 8.00. Similar results have been reported before at 37 °C,[6] and very recently at room temperature.[34] Consequently, Figure 1B shows that the estimated value of k_{on} decreases as pH is increased, suggesting that the binding of H_2S to Mb-Fe^{III} is kinetically favored as compared to its conjugated base, HS^-.

A similar procedure was used with NAcMP11-Fe^{III}. In this case, the pH interval selected was limited to 5.60−7.10, in

order to avoid spurious reactions interfering at higher pHs. Evidences of the fast formation of polysulfides at alkaline pH have been reported;[59−61] the putative formation of bound polysulfide species was discarded in our experiments, according to reported data.[62] The formation of polysulfides is associated with the subsequent formation of sulfur, which hinders the absorbance measurements and minor quantities are observed at all pH values. To avoid this inconvenience, the reaction was carried out in the limit or below the pseudo-first-order conditions. In the pH interval selected and controlling the ratio [NAcMP11-Fe^{III}]/[Na$_2$S], no reduction Fe^{III}/Fe^{II} was observed during data acquisition (Supporting Information section SI3), and the resulting process was attributed only to the binding of sulfide species to Fe^{III}, previously characterized at pH 6.8.[11] With these constraints, Figure 2A,B were obtained in

Figure 2. NAcMP11-Fe^{III}-sulfide complex formation as a function of pH. (A) Representative stopped flow measurements at λ_{max}= 398 nm. (B) k_{obs} as a function of Na$_2$S concentration. The k_{on} values at each pH are obtained from the slopes of each linear dependence; the k_{on} (in M^{-1} s^{-1}) values obtained are (0.33 ± 0.07) × 10^4 at pH 5.60 (black circles), (0.49 ± 0.09) × 10^4 at pH 5.90 (red squares), (0.68 ± 0.16) × 10^4 at pH 6.10 (blue triangles), (0.78 ± 0.10) × 10^4 at pH 6.30 (green small circles), (1.5 ± 0.3) × 10^4 at pH 6.70 (yellow empty squares), (1.8 ± 0.2) × 10^4 at pH 6.90 (brown empty circles), and (1.9 ± 0.3) × 10^4 at pH 7.1(cyan empty triangles).

functions, and the fast process was analyzed to derive k_{obs}. The slow process was attributed to secondary reactions, probably including ligand release.[63]

The plots of k_{obs} versus varying concentrations of Na$_2$S solutions allowed the estimation of the binding constants, k_{on}, at each pH from the slopes of the linear fitted data. A linear dependence of the reaction rates at each pH with the concentration of sulfide is observed for Mb-Fe^{III} and NAcMP11-Fe^{III}, indicating second-order kinetics for the binding processes. Opposite to the tendency for Mb-Fe^{III}, minimalistic NAcMP11-Fe^{III} model compound shows an increase in the rate of the binding to sulfide species as pH is increased from 5.60 to 7.10 (Figure 2A), and the corresponding k_{on} values derived from the kinetic traces increase with pH (Figure 2B). The values of k_{on} near pH 7 are in agreement with those previously reported[11,34] and vary only within 1 order of magnitude in the pH intervals evaluated for Mb-Fe^{III} and NAcMP11-Fe^{III}, regardless the sign of the variation. The order of magnitude of the values of k_{on} lay within the range of those reported for over 40 hemeprotein systems toward inorganic sulfide (Supporting Information section SI1). Collectively, these results strongly point at a common dissociative mechanism, with the release of the bound water molecule as the rate limiting step of the process.[64−66] As stated above, the decrease of k_{on} as a function of pH has been previously reported for Mb-Fe^{III},[6,33,34] for Hb I, II, and III from *Lucina pectinata*,[3] for Hb from *Vitreoscilla*,[4] and for human[5,33] and porcine hemoglobins.[34]

In order to dissect the reactivity of H$_2$S and HS$^-$ in the binding to the metal center we used eq 2 (Experimental Section) for the analytical estimation of the intrinsic kinetic rate constants for H$_2$S and HS$^-$, with the set of k_{on} versus pH values derived from Figures 1B and 2B. For the case of Mb-Fe^{III}, the use of complete eq 2 yields a value for $k_{int}^{HS^-}$ that does not differ significantly or statistically from zero. We used the eq 4 as a simplified version of eq 2, assuming $k_{int}^{HS^-}$ is negligible. Both equations yield a similar value for $k_{int}^{H_2S}$ (Supporting Information section SI5). Hence, we assumed that only H$_2$S is capable of effectively binding the iron center.

$$k_{on} = \frac{k_{int}^{H_2S} \cdot 10^{-pH}}{(K_a + 10^{-pH})} \tag{4}$$

For the calculation of the intrinsic rate constants for the binding of H$_2$S or HS$^-$ to NAcMP11-Fe^{III}, we used complete eq 2, similar to the procedure used with Mb-Fe^{III} data set. The results are included in Table 1, and indicate that while H$_2$S is

Table 1. Values of k_{int} for H$_2$S and HS$^-$ in the Binding to Mb-Fe^{III} or NAcMP11-Fe^{III}

	Mb-Fe^{III} estimate (±std. error) M^{-1} s^{-1}	NAcMP11-Fe^{III} estimate (±std. error) M^{-1} s^{-1}
$k_{int}^{H_2S}$	3.12 (±0.27) × 10^4	2.61 (±0.63) × 10^3
$k_{int}^{HS^-}$		3.42 (±0.15) × 10^4

a similar way than those for Mb-Fe^{III}, although data are more dispersed. Figure 2A shows the variation of the decay of the starting NAcMP11-Fe^{III} as a function of pH, after rapid mixing with Na$_2$S solution ([NAcMP11-Fe^{III}]:[S] = 1:80). No significant formation of polysulfides was detected in these experiments. The decays were fitted with double exponential

the unique binding species of sulfide toward Mb-Fe^{III}, in agreement with a very recent report,[33] HS$^-$ appears as the main binding species when the ferric heme is accessed with no distal impediment, except that of the water molecule blocking the binding site. Furthermore, the binding of either H$_2$S or HS$^-$ is significant for the model NAcMP11-Fe^{III}, being that of

the monoanionic species almost 30 fold faster compared to the neutral one.

The K_{a1} value ($2.15 \times 10^{-7} \pm 4.06 \times 10^{-8}$) for H$_2$S was derived from the analysis for the case of Mb-Fe^{III}, and is in good accordance with the value reported. For the case of NAcMP11-Fe^{III}, we improved the fitting of the data set by using a reported value for $K_{a1} = 1.1 \times 10^{-7}$.[56]

The values of k_{on} for the binding of sulfide to Mb-Fe^{III} or NAcMP11-Fe^{III} as a function of pH are presented in Figure 3. The black curves show the fitting to eq 2. An inverse preference for the binding of sulfide species to the selected heme structures is evidenced in the pH intervals studied.
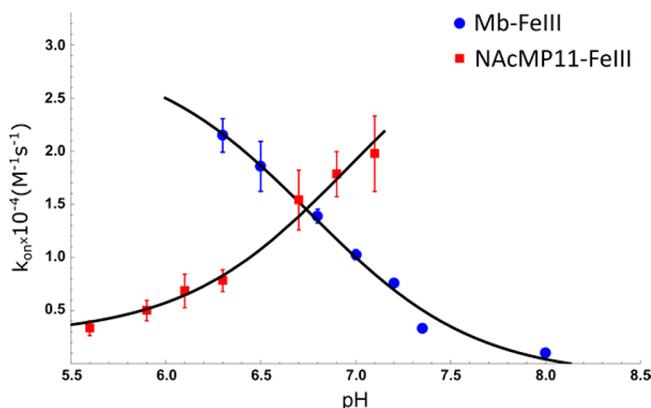

Figure 3. Plot of k_{on} as a function of pH for the reaction of Mb-Fe^{III} (blue dots) or NAcMP11-Fe^{III} (red squares) and Na$_2$S solutions.

The pH dependence of the reaction rate depicts single ionization processes for both cases, with an inflection point near the pK_{a1} of H$_2$S. Contrary to the expectation for a dissociative binding mechanism operating in both systems that would yield similar binding constants for any ligand, the experimental k_{int} for HS$^-$ surpasses that of H$_2$S in the case of NAcMP11-Fe^{III}.

To further explain the kinetic results summarized in Figure 3, a detailed inspection of the systems behavior was performed by computational methods. Molecular dynamics simulation techniques, specifically, the combination of sMD and the Jarzynski equality were used. The methodology provides the molecular details of the migration process of sulfide species in Mb-Fe^{III} and in MP11-Fe^{III}, and has been successfully applied to other studies in proteins.[10,67]

The results derived from the sMD simulations for Mb-Fe^{III} show that the free energy profile associated with the migration of H$_2$S presents a low barrier of about 1 kcal/mol (Figure 4, upper panel) with almost zero free energy difference between the bulk and the active site. Conversely, HS$^-$ displays a high barrier (~7 kcal/mol) and a free energy difference between the bulk solvent and the active site of approximately 6 kcal/mol. The profiles are ended at 4.5 Å from the iron atom, as the classical force field used is not able to describe the electronic interaction during Fe−S bond formation. These results show that H$_2$S is the most favorable species to migrate from the bulk to the active site of Mb-Fe^{III} in agreement with the measured intrinsic constant. A simple estimation of the ratio between the experimental intrinsic constants is in accordance with the difference in the energy barriers derived from the sMD analysis, pointing at the migration of HS$^-$ as restraining its
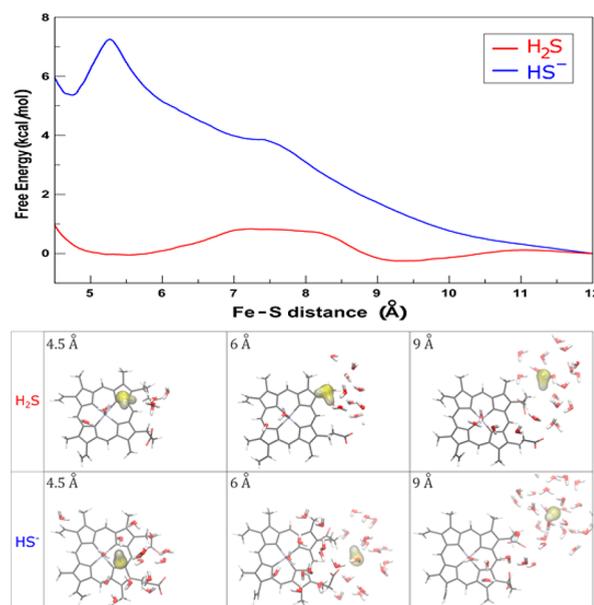
Figure 4. Upper panel: free energy profiles (red and blue for H$_2$S and HS$^-$, respectively) for ligand migration through E7-gate in Mb-Fe^{III}. Lower panels: representative structures of sMD trajectories at 4.5, 6, and 9 Å of reaction coordinate for H$_2$S and HS$^-$.

overall binding process. Experimentally, as stated above, this is reflected in the result obtained for $k_{int (HS^-)}$.

The difference between the two free energy profiles can be rationalized by inspecting the individual sMD trajectories for both ligands. When H$_2$S migrates through the E7 pathway from the bulk to the active site its solvation structure changes dramatically, expelling water molecules from its surroundings almost completely upon reaching the active site (Figure 4, lower panel). On the contrary, HS$^-$ migrates to the active site partially solvated, most likely due to its net charge. Consequently, the energy profile reveals a barrier ascribed to a high desolvation cost in the access of the binding site. For both ligands, the minimum in the free energy profile located at ~5 Å was attributed to the hydrogen bond stabilization of the migrating ligand by a coordinated water molecule and HisE7.[10]

Remarkably, the HisE7 (histidine-gate tunnel) does not seem to affect dramatically the migration of the sulfide ligands. In fact, for both sulfide ligands, the hydrogen bond stabilization by HisE7 takes place after the desolvation process occurs. This type of mechanism where the HisE7 does not participate as a gate but more likely provides a mechanism for the stabilization of the ligand, has been reported before.[7,25]

The results for the sMD analysis for MP11-Fe^{III} are presented in Figure 5. The free energy profiles show barriers of about 0.5 and 2.5 kcal/mol for the migration toward the heme in NAcMP11-Fe^{III}, for H$_2$S and HS$^-$ respectively. This can be ascribed to a partial desolvation process of the HS$^-$ anion in the surroundings of the heme moiety.

The variations in free energy barriers are lower than those obtained for Mb-Fe^{III} for each ligand, highlighting that the absence of the protein tunnels and cavities allows both ligands to reach the metal center. Of note is that the results obtained in the sMD simulation suggest an opposite kinetic behavior than the experimental results; hence, the migration is not controlling the process of binding of H$_2$S nor HS$^-$, contrasting with the behavior of the anionic ligand in the Mb-Fe^{III} case. Taken together, the results suggest that additional processes
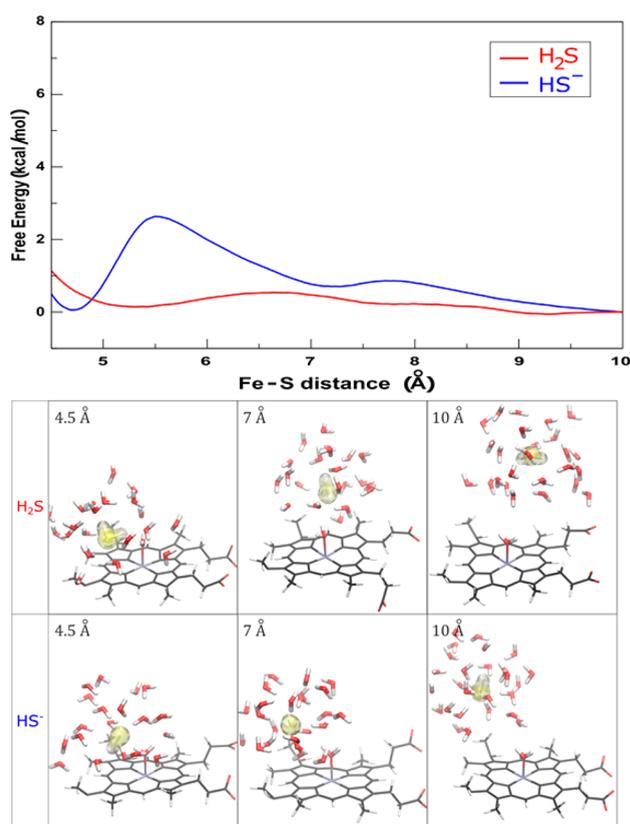
Figure 5. Upper panel: free energy profiles (red and blue for H$_2$S and HS$^-$ respectively) for ligand binding to NAcMP**11**-Fe^{III}. Lower panels: representative structure of sMD trajectories at 4.5, 7, and 10 Å of reaction coordinate for H$_2$S and HS$^-$.

should be taken into account to describe the binding of sulfide species to NAcMP**11**-Fe^{III}. It can be hypothesized that (1) there must be a barrier after migration (distance Fe−S < 5 Å) that favors HS$^-$ and/or that (2) the binding mechanism has a significant associative character. In this last scenario, the experimental results can be ascribed to the higher nucleophilicity of HS$^-$.[68]

The values obtained for the highest occupied molecular orbital HOMO, a usual indicator of nucleophilicity, for the anionic and neutral species are $E_{HOMO(HS^-)}$ = −7.1 eV, and $E_{HOMO(H_2S)}$ = −9.4 eV, respectively. As expected, E_{HOMO} is more negative for H$_2$S, suggesting a lower nucleophilicity, even if the compound still behaves as a nucleophile toward the ferric heme centers. This is further supported by the absence of distal mechanisms of stabilization of the water molecule in the NAcMP**11**-Fe^{III}, favoring associative processes as compared to the Mb-Fe^{III}. An associative character has been envisioned in the studies of the binding of cysteine/cysteinate[69] or hydrogen cyanide/cyanide toward microperoxidase peptides.[29,70] Furthermore, while the cysteine/cysteinate and hydrogen cyanide/cyanide pairs have only one effectively binding species (namely, cysteinate and cyanide), both H$_2$S and HS$^-$ can bind ferric heme compounds.

Further analysis for the k_{on} for sulfide binding to ferric hemeproteins (Supporting Information section SI1) with a sixth coordinated water molecule, often stabilized by distal mechanisms, indicates that the protein matrix favors the weak nucleophile H$_2$S, and that the binding mechanism is conceivably dissociative. If the stabilization of the water

molecule is weak or absent as in MP**11**, then the intrinsic chemical features of H$_2$S and HS$^-$ would be ruling the binding mechanism.

■ CONCLUSIONS

We provide evidence regarding the impact of the acid−base equilibria of H$_2$S and its conjugated base HS$^-$ on the migration and binding of sulfide species to the holoprotein Mb-Fe^{III} and the model compound NAcMP**11**-Fe^{III}. A dissociative mechanism for the binding of H$_2$S to Mb-Fe^{III} is conceivably operating according to the k_{on} values in the range of pHs tested with the release of a coordinated water molecule as the rate-limiting step. The prevalence of H$_2$S in the binding to Mb-Fe^{III} is explained in terms of the desolvation cost for the HS$^-$ charged species in the course of the migration process, which hampers the access of the solvated anion to the active site.

Conversely, the access for either H$_2$S or HS$^-$ to the binding site of MP**11**-Fe^{III} is not significantly affected by migration filters. Despite a desolvation cost, the preferred binding of the monoanionic species HS$^-$ to NAcMP**11**-Fe^{III} is experimentally observed and exceeds the binding of the neutral H$_2$S. An associative character of the binding mechanism of HS$^-$ is plausible to account for the difference. The associative component can be ascribed to the higher nucleophilicity of the HS$^-$ ligand for the reaction with a Fe^{III}(H$_2$O) devoid of stabilization by distal mechanisms.

The systems selected allow the dissection of the steps composing the binding process, namely the migration and intrinsic binding mechanisms. When a protein matrix has hydrophobic migration channels as compared to the bulk, the access of the HS$^-$ charged species is likely restricted. In the absence of access restrictions, both species can reach the proximity of the binding site and effectively bind the ferric ion, being the most nucleophilic HS$^-$ the preferred ligand.

The reaction of H$_2$S/HS$^-$ toward NAcMP**11**-Fe^{III} is the first example where the intrinsic binding constants have been determined for both conjugated ligands, and disclose aspects of the reaction mechanism. Overall, the combination of experimental and computational procedures suggests that both species can bind the ferric heme compounds, and the binding of HS$^-$, if accessing a hemeprotein binding site, is favored over H$_2$S.

■ ASSOCIATED CONTENT

Ⓢ Supporting Information

The Supporting Information is available free of charge on the ACS Publications website at DOI: 10.1021/acs.inorgchem.8b00478.

Compilation of reported sulfide binding rate constants to ferric heme compounds, the structure of microperoxidase **11**, the sets of UV−vis spectra derived from the stopped flow experiments at different pHs, technical details of the convergence of steered molecular dynamics simulations and free energy estimations, and complete kinetic model employed for the analysis (PDF)

■ AUTHOR INFORMATION

Corresponding Author
* bari@qi.fcen.uba.ar.

ORCID Ⓘ
Darío A. Estrin: 0000-0002-5006-7225
Sara E. Bari: 0000-0003-1604-6196

■ REFERENCES

(1) Sulfide or inorganic sulfide species (S) refer to the sum of the conjugated species hydrogen sulfide (H_2S), hydrosulfide (HS^-), and sulfide (S^{2-}).

(2) Pavlik, J. W.; Noll, B. C.; Oliver, A. G.; Schulz, C. E.; Scheidt, W. R. Hydrosulfide (HS^-) Coordination in Iron Porphyrinates. *Inorg. Chem.* **2010**, *49* (3), 1017−1026.

(3) Kraus, D. W.; Wittenberg, J. B. Hemoglobins of the Lucina Pectinata/Bacteria Symbiosis. I. Molecular Properties, Kinetics and Equilibria of Reactions with Ligands. *J. Biol. Chem.* **1990**, *265* (27), 16043−16053.

(4) Wang, D.; Liu, L.; Wang, H.; Xu, H.; Chen, L.; Ma, L.; Li, Z. Clues for Discovering a New Biological Function of *Vitreoscilla* Hemoglobin in Organisms: Potential Sulfide Receptor and Storage. *FEBS Lett.* **2016**, *590* (8), 1132−1142.

(5) Vitvitsky, V.; Yadav, P. K.; Kurthen, A.; Banerjee, R. Sulfide Oxidation by a Noncanonical Pathway in Red Blood Cells Generates Thiosulfate and Polysulfides. *J. Biol. Chem.* **2015**, *290* (13), 8310−8320.

(6) Bostelaar, T.; Vitvitsky, V.; Kumutima, J.; Lewis, B. E.; Yadav, P. K.; Brunold, T. C.; Filipovic, M.; Lehnert, N.; Stemmler, T. L.; Banerjee, R. Hydrogen Sulfide Oxidation by Myoglobin. *J. Am. Chem. Soc.* **2016**, *138* (27), 8476−8488.

(7) Boechi, L.; Arrar, M.; Martí, M. A.; Olson, J. S.; Roitberg, A. E.; Estrin, D. A. Hydrophobic Effect Drives Oxygen Uptake in Myoglobin via Histidine E7. *J. Biol. Chem.* **2013**, *288* (9), 6754−6762.

(8) Pietri, R.; Lewis, A.; León, R. G.; Casabona, G.; Kiger, L.; Yeh, S.-R.; Fernandez-Alberti, S.; Marden, M. C.; Cadilla, C. L.; López-Garriga, J. Factors Controlling the Reactivity of Hydrogen Sulfide with Hemeproteins. *Biochemistry* **2009**, *48* (22), 4881−4894.

(9) Pietri, R.; León, R. G.; Kiger, L.; Marden, M. C.; Granell, L. B.; Cadilla, C. L.; López-Garriga, J. Hemoglobin I from Lucina Pectinata: A Model for Distal Heme-Ligand Control. *Biochim. Biophys. Acta, Proteins Proteomics* **2006**, *1764* (4), 758−765.

(10) Boubeta, F. M.; Bari, S. E.; Estrin, D. A.; Boechi, L. Access and Binding of H_2S to Hemeproteins: The Case of HbI of *Lucina Pectinata. J. Phys. Chem. B* **2016**, *120* (36), 9642−9653.

(11) Bieza, S. A.; Boubeta, F.; Feis, A.; Smulevich, G.; Estrin, D. A.; Boechi, L.; Bari, S. E. Reactivity of Inorganic Sulfide Species toward a Heme Protein Model. *Inorg. Chem.* **2015**, *54* (2), 527−533.

(12) Watanabe, K.; Suzuki, T.; Kitagishi, H.; Kano, K. Reaction between a Haemoglobin Model Compound and Hydrosulphide in Aqueous Solution. *Chem. Commun.* **2015**, *51* (19), 4059−4061.

(13) Zhao, Z.; Wang, D.; Wang, M.; Sun, X.; Wang, L.; Huang, X.; Ma, L.; Li, Z. Proximal Environment Controlling the Reactivity between Inorganic Sulfide and Heme-Peptide Model. *RSC Adv.* **2016**, *6* (82), 78858−78864.

(14) Milani, M. Mycobacterium Tuberculosis Hemoglobin N Displays a Protein Tunnel Suited for O2 Diffusion to the Heme. *EMBO J.* **2001**, *20* (15), 3902−3909.

(15) Elber, R. Ligand Diffusion in Globins: Simulations versus Experiment. *Curr. Opin. Struct. Biol.* **2010**, *20* (2), 162−167.

(16) Perutz, M. F.; Mathews, F. S. An X-Ray Study of Azide Methaemoglobin. *J. Mol. Biol.* **1966**, *21* (1), 199−202.

(17) Scott, E. E.; Gibson, Q. H.; Olson, J. S. Mapping the Pathways for O_2 Entry Into and Exit from Myoglobin. *J. Biol. Chem.* **2001**, *276* (7), 5177−5188.

(18) Brunori, M. Structural Dynamics of Myoglobin. *Biophys. Chem.* **2000**, *86* (2−3), 221−230.

(19) Brunori, M.; Vallone, B.; Cutruzzola, F.; Travaglini-Allocatelli, C.; Berendzen, J.; Chu, K.; Sweet, R. M.; Schlichting, I. The Role of Cavities in Protein Dynamics: Crystal Structure of a Photolytic Intermediate of a Mutant Myoglobin. *Proc. Natl. Acad. Sci. U. S. A.* **2000**, *97* (5), 2058−2063.

(20) Milani, M.; Pesce, A.; Ouellet, Y.; Dewilde, S.; Friedman, J.; Ascenzi, P.; Guertin, M.; Bolognesi, M. Heme-Ligand Tunneling in Group I Truncated Hemoglobins. *J. Biol. Chem.* **2004**, *279* (20), 21520−21525.

(21) Mishra, S.; Meuwly, M. Nitric Oxide Dynamics in Truncated Hemoglobin: Docking Sites, Migration Pathways, and Vibrational Spectroscopy from Molecular Dynamics Simulations. *Biophys. J.* **2009**, *96* (6), 2105−2118.

(22) Ouellet, Y. H.; Daigle, R.; Lagüe, P.; Dantsker, D.; Milani, M.; Bolognesi, M.; Friedman, J. M.; Guertin, M. Ligand Binding to Truncated Hemoglobin N from *Mycobacterium Tuberculosis* Is Strongly Modulated by the Interplay between the Distal Heme Pocket Residues and Internal Water. *J. Biol. Chem.* **2008**, *283* (40), 27270−27278.

(23) Goldbeck, R. A.; Bhaskaran, S.; Ortega, C.; Mendoza, J. L.; Olson, J. S.; Soman, J.; Kliger, D. S.; Esquerra, R. M. Water and Ligand Entry in Myoglobin: Assessing the Speed and Extent of Heme Pocket Hydration after CO Photodissociation. *Proc. Natl. Acad. Sci. U. S. A.* **2006**, *103* (5), 1254−1259.

(24) Olson, J. S.; Phillips, G. N. Myoglobin Discriminates between O2, NO, and CO by Electrostatic Interactions with the Bound Ligand. *JBIC, J. Biol. Inorg. Chem.* **1997**, *2* (4), 544−552.

(25) Bustamante, J. P.; Abbruzzetti, S.; Marcelli, A.; Gauto, D.; Boechi, L.; Bonamore, A.; Boffi, A.; Bruno, S.; Feis, A.; Foggi, P.; et al. Ligand Uptake Modulation by Internal Water Molecules and Hydrophobic Cavities in Hemoglobins. *J. Phys. Chem. B* **2014**, *118* (5), 1234−1245.

(26) Bustamante, J. P.; Szretter, M. E.; Sued, M.; Martí, M. A.; Estrin, D. A.; Boechi, L. A Quantitative Model for Oxygen Uptake and Release in a Family of Hemeproteins. *Bioinformatics* **2016**, *32* (12), 1805−1813.

(27) Cerda, J.; Echevarria, Y.; Morales, E.; López-Garriga, J. Resonance Raman Studies of the Heme-Ligand Active Site of Hemoglobin I FromLucina Pectinata. *Biospectroscopy* **1999**, *5* (5), 289−301.

(28) Nicoletti, F. P.; Comandini, A.; Bonamore, A.; Boechi, L.; Boubeta, F. M.; Feis, A.; Smulevich, G.; Boffi, A. Sulfide Binding Properties of Truncated Hemoglobins. *Biochemistry* **2010**, *49* (10), 2269−2278.

(29) Ascenzi, P.; Sbardella, D.; Santucci, R.; Coletta, M. Cyanide Binding to Ferrous and Ferric Microperoxidase-11. *JBIC, J. Biol. Inorg. Chem.* **2016**, *21* (4), 511−522.

(30) Dou, Y.; Olson, J. S.; Wilkinson, A. J.; Ikeda-Saito, M. Mechanism of Hydrogen Cyanide Binding to Myoglobin. *Biochemistry* **1996**, *35* (22), 7107−7113.

(31) Pálinkás, Z.; Furtmüller, P. G.; Nagy, A.; Jakopitsch, C.; Pirker, K. F.; Magierowski, M.; Jasnos, K.; Wallace, J. L.; Obinger, C.; Nagy, P. Interactions of Hydrogen Sulfide with Myeloperoxidase: Sulfide Is a Substrate and Inhibitor of Myeloperoxidase. *Br. J. Pharmacol.* **2015**, *172* (6), 1516−1532.

(32) Hartle, M. D.; Prell, J. S.; Pluth, M. D. Spectroscopic Investigations into the Binding of Hydrogen Sulfide to Synthetic Picket-Fence Porphyrins. *Dalton Trans.* **2016**, *45* (11), 4843−4853.

(33) Jensen, B.; Fago, A. Reactions of Ferric Hemoglobin and Myoglobin with Hydrogen Sulfide under Physiological Conditions. *J. Inorg. Biochem.* **2018**, *182*, 133−140.

(34) Mot, A. C.; Bischin, C.; Damian, G.; Attia, A. A. A.; Gal, E.; Dina, N.; Leopold, N.; Silaghi-Dumitrescu, R. Fe(III) − Sulfide Interaction in Globins: Characterization and Quest for a Putative Fe(IV)-Sulfide Species. *J. Inorg. Biochem.* **2018**, *179*, 32−39.

(35) Marques, H. M. Insights into Porphyrin Chemistry Provided by the Microperoxidases, the Haempeptides Derived from Cytochrome C. *Dalton Trans.* **2007**, No. 39, 4371.

(36) Carraway, A. D.; Povlock, S. L.; Houston, M. L.; Johnston, D. S.; Peterson, J. Monomeric Ferric Heme Peptide Derivatives: Model Systems for Hemoproteins. *J. Inorg. Biochem.* **1995**, *60* (4), 267−276.

(37) Marques, H.; Perry, C. Hemepeptide Models for Hemoproteins: The Behavior of -Acetylmicroperoxidase-11 in Aqueous Solution. *J. Inorg. Biochem.* **1999**, *75* (4), 281−291.

(38) *Mathematica*, version 10.4; Wolfram Research Inc: Champaign, IL, 2016.

(39) Case, D. A.; Babin, V.; Berryman, J. T.; Betz, R. M.; Cai, Q.; Cerutti, D. S.; Cheatham, T. E., III; Darden, T. A.; Duke, R. E.; Gohlke, H. et al. *AMBER 14*; University of California: San Francisco, CA, 2014.

(40) Lindorff-Larsen, K.; Piana, S.; Palmo, K.; Maragakis, P.; Klepeis, J. L.; Dror, R. O.; Shaw, D. E. Improved Side-Chain Torsion Potentials for the Amber Ff99SB Protein Force Field. *Proteins: Struct., Funct., Genet.* **2010**, 1950−1958.

(41) Frisch, M. J.; Trucks, G. W.; Schlegel, H. B.; Scuseria, G. E.; Robb, M. A.; Cheeseman, J. R.; Montgomery, J. A., Jr.; Vreven, T.; Kudin, K. N.; Burant, J. C.; Millam, J. M.; Iyengar, S. S.; Tomasi, J.; Barone, V.; Mennucci, B.; Cossi, M.; Scalmani, G.; Rega, N.; Petersson, G. A.; Nakatsuji, H.; Hada, M.; Ehara, M.; Toyota, K.; Fukuda, R.; Hasegawa, J.; Ishida, M.; Nakajima, T.; Honda, Y.; Kitao, O.; Nakai, H.; Klene, M.; Li, X.; Knox, J. E.; Hratchian, H. P.; Cross, J. B.; Bakken, V.; Adamo, C.; Jaramillo, J.; Gomperts, R.; Stratmann, R. E.; Yazyev, O.; Austin, A. J.; Cammi, R.; Pomelli, C.; Ochterski, J. W.; Ayala, P. Y.; Morokuma, K.; Voth, G. A.; Salvador, P.; Dannenberg, J. J.; Zakrzewski, V. G.; Dapprich, S.; Daniels, A. D.; Strain, M. C.; Farkas, O.; Malick, D. K.; Rabuck, A. D.; Raghavachari, K.; Foresman, J. B.; Ortiz, J. V.; Cui, Q.; Baboul, A. G.; Clifford, S.; Cioslowski, J.; Stefanov, B. B.; Liu, G.; Liashenko, A.; Piskorz, P.; Komaromi, I.; Martin, R. L.; Fox, D. J.; Keith, T.; Al-Laham, M. A.; Peng, C. Y.; Nanayakkara, A.; Challacombe, M.; Gill, P. M. W.; Johnson, B.; Chen, W.; Wong, M. W.; Gonzalez, C.; Pople, J. A. *Gaussian 03*, revision C.02; Gaussian, Inc.: Wallingford, CT, 2004.

(42) Soldatova, A. V.; Ibrahim, M.; Olson, J. S.; Czernuszewicz, R. S.; Spiro, T. G. New Light on NO Bonding in Fe(III) Heme Proteins from Resonance Raman Spectroscopy and DFT Modeling. *J. Am. Chem. Soc.* **2010**, *132* (13), 4614−4625.

(43) Marti, M. A.; Crespo, A.; Capece, L.; Boechi, L.; Bikiel, D. E.; Scherlis, D. A.; Estrin, D. A. Dioxygen Affinity in Heme Proteins Investigated by Computer Simulation. *J. Inorg. Biochem.* **2006**, *100* (4), 761−770.

(44) Capece, L.; Marti, M. A.; Crespo, A.; Doctorovich, F.; Estrin, D. A. Heme Protein Oxygen Affinity Regulation Exerted by Proximal Effects. *J. Am. Chem. Soc.* **2006**, *128* (38), 12455−12461.

(45) Marti, M. A.; Capece, L.; Bidon-Chanal, A.; Crespo, A.; Guallar, V.; Luque, F. J.; Estrin, D. A. Nitric Oxide Reactivity with Globins as Investigated Through Computer Simulation. *Methods Enzymol.* **2008**, *437*, 477−498.

(46) Martí, M. A.; Capece, L.; Bikiel, D. E.; Falcone, B.; Estrin, D. A. Oxygen Affinity Controlled by Dynamical Distal Conformations: The Soybean Leghemoglobin and the Paramecium Caudatum Hemoglobin Cases. *Proteins: Struct., Funct., Genet.* **2007**, *68* (2), 480−487.

(47) Perdew, J. P.; Burke, K.; Ernzerhof, M. Generalized Gradient Approximation Made Simple. *Phys. Rev. Lett.* **1996**, *77* (18), 3865−3868.

(48) Nadra, A. D.; Martí, M. A.; Pesce, A.; Bolognesi, M.; Estrin, D. A. Exploring the Molecular Basis of Heme Coordination in Human Neuroglobin. *Proteins: Struct., Funct., Genet.* **2008**, *71* (2), 695−705.

(49) Howes, B. D.; Giordano, D.; Boechi, L.; Russo, R.; Mucciacciaro, S.; Ciaccio, C.; Sinibaldi, F.; Fittipaldi, M.; Martí, M. A.; Estrin, D. A.; et al. The Peculiar Heme Pocket of the 2/2 Hemoglobin of Cold-Adapted Pseudoalteromonas Haloplanktis TAC125. *JBIC, J. Biol. Inorg. Chem.* **2011**, *16* (2), 299−311.

(50) Capece, L.; Lewis-Ballester, A.; Yeh, S.-R.; Estrin, D. A.; Marti, M. A. Complete Reaction Mechanism of Indoleamine 2,3-Dioxygenase as Revealed by QM/MM Simulations. *J. Phys. Chem. B* **2012**, *116* (4), 1401−1413.

(51) Arroyo Mañez, P.; Lu, C.; Boechi, L.; Martí, M. A.; Shepherd, M.; Wilson, J. L.; Poole, R. K.; Luque, F. J.; Yeh, S.-R.; Estrin, D. A. Role of the Distal Hydrogen-Bonding Network in Regulating Oxygen Affinity in the Truncated Hemoglobin III from *Campylobacter Jejuni*. *Biochemistry* **2011**, *50* (19), 3946−3956.

(52) Bidon-Chanal, A.; Martí, M. A.; Crespo, A.; Milani, M.; Orozco, M.; Bolognesi, M.; Luque, F. J.; Estrin, D. A. Ligand-Induced Dynamical Regulation of NO Conversion in Mycobacterium Tuberculosis Truncated Hemoglobin-N. *Proteins: Struct., Funct., Genet.* **2006**, *64* (2), 457−464.

(53) Oliveira, A.; Singh, S.; Bidon-Chanal, A.; Forti, F.; Martí, M. A.; Boechi, L.; Estrin, D. A.; Dikshit, K. L.; Luque, F. J. Role of PheE15 Gate in Ligand Entry and Nitric Oxide Detoxification Function of Mycobacterium Tuberculosis Truncated Hemoglobin N. *PLoS One* **2012**, *7* (11), e49291.

(54) Boechi, L.; Martí, M. A.; Milani, M.; Bolognesi, M.; Luque, F. J.; Estrin, D. A. Structural Determinants of Ligand Migration in Mycobacterium Tuberculosis Truncated Hemoglobin O. *Proteins: Struct., Funct., Genet.* **2008**, *73* (2), 372−379.

(55) Chai, J.-D.; Head-Gordon, M. Long-Range Corrected Hybrid Density Functionals with Damped Atom−atom Dispersion Corrections. *Phys. Chem. Chem. Phys.* **2008**, *10* (44), 6615.

(56) Sun, W.; Nešić, S.; Young, D.; Woollam, R. C. Equilibrium Expressions Related to the Solubility of the Sour Corrosion Product Mackinawite. *Ind. Eng. Chem. Res.* **2008**, *47* (5), 1738−1742.

(57) Li, Q.; Lancaster, J. R. Chemical Foundations of Hydrogen Sulfide Biology. *Nitric Oxide* **2013**, *35*, 21−34.

(58) Traylor, T. G.; Deardurff, L. A.; Coletta, M.; Ascenzi, P.; Antonini, E.; Brunori, M. Reactivity of Ferrous Heme Proteins at Low pH. *J. Biol. Chem.* **1983**, *258* (20), 12147−12148.

(59) Giggenbach, W. Optical Spectra and Equilibrium Distribution of Polysulfide Ions in Aqueous Solution at 20.Deg. *Inorg. Chem.* **1972**, *11* (6), 1201−1207.

(60) Nagy, P. Mechanistic Chemical Perspective of Hydrogen Sulfide Signaling. *Methods Enzymol.* **2015**, *554*, 3−29.

(61) Nagy, P.; Pálinkás, Z.; Nagy, A.; Budai, B.; Tóth, I.; Vasas, A. Chemical Aspects of Hydrogen Sulfide Measurements in Physiological Samples. *Biochim. Biophys. Acta, Gen. Subj.* **2014**, *1840* (2), 876−891.

(62) Galardon, E.; Huguet, F.; Herrero, C.; Ricoux, R.; Artaud, I.; Padovani, D. Reactions of Persulfides with the Heme Cofactor of Oxidized Myoglobin and Microperoxidase 11: Reduction or Coordination. *Dalton Trans.* **2017**, *46* (24), 7939−7946.

(63) Ruetz, M.; Kumutima, J.; Lewis, B. E.; Filipovic, M. R.; Lehnert, N.; Stemmler, T. L.; Banerjee, R. A Distal Ligand Mutes the Interaction of Hydrogen Sulfide with Human Neuroglobin. *J. Biol. Chem.* **2017**, *292* (16), 6512−6528.

(64) Laverman, L. E.; Ford, P. C. Mechanistic Studies of Nitric Oxide Reactions with Water Soluble Iron(II), Cobalt(II), and Iron(III) Porphyrin Complexes in Aqueous Solutions: Implications for Biological Activity. *J. Am. Chem. Soc.* **2001**, *123* (47), 11614−11622.

(65) Polticelli, F.; Zobnina, V.; Ciaccio, C.; de Sanctis, G.; Ascenzi, P.; Coletta, M. Enhanced Heme Accessibility in Horse Heart Mini-Myoglobin: Insights from Molecular Modelling and Reactivity Studies. *Arch. Biochem. Biophys.* **2015**, *585*, 1−9.

(66) De Sanctis, G.; Petrella, G.; Ciaccio, C.; Feis, A.; Smulevich, G.; Coletta, M. A Comparative Study on Axial Coordination and Ligand Binding in Ferric Mini Myoglobin and Horse Heart Myoglobin. *Biophys. J.* **2007**, *93* (6), 2135−2142.

(67) Forti, F.; Boechi, L.; Estrin, D. A.; Marti, M. A. Comparing and Combining Implicit Ligand Sampling with Multiple Steered Molecular Dynamics to Study Ligand Migration Processes in Heme Proteins. *J. Comput. Chem.* **2011**, *32* (10), 2219−2231.

(68) Cuevasanta, E.; Lange, M.; Bonanata, J.; Coitiño, E. L.; Ferrer-Sueta, G.; Filipovic, M. R.; Alvarez, B. Reaction of Hydrogen Sulfide with Disulfide and Sulfenic Acid to Form the Strongly Nucleophilic Persulfide. *J. Biol. Chem.* **2015**, *290* (45), 26866−26880.

(69) Zhong, F.; Lisi, G. P.; Collins, D. P.; Dawson, J. H.; Pletneva, E. V. Redox-Dependent Stability, Protonation, and Reactivity of Cysteine-Bound Heme Proteins. *Proc. Natl. Acad. Sci. U. S. A.* **2014**, *111* (3), E306−E315.

(70) Marques, H. M. Peroxidase Activity of the Hemeoctapeptide *N*-Acetylmicroperoxidase-8. *Inorg. Chem.* **2005**, *44* (18), 6146−6148.